



Analysis of the Flow Interactions between Large Water Droplets and Air in Droplet Acceleration Nozzles

P. A. Kessel
ARO, Inc.

May 1980

Final Report for Period October 1978 — September 1979

**TECHNICAL REPORTS
FILE COPY**

Approved for public release, distribution unlimited.

Property of U. S. Air Force
AEDC LIBRARY
F40600-77-C-0003

**ARNOLD ENGINEERING DEVELOPMENT CENTER
ARNOLD AIR FORCE STATION, TENNESSEE
AIR FORCE SYSTEMS COMMAND
UNITED STATES AIR FORCE**

NOTICES

When U. S. Government drawings, specifications, or other data are used for any purpose other than a definitely related Government procurement operation, the Government thereby incurs no responsibility nor any obligation whatsoever, and the fact that the Government may have formulated, furnished, or in any way supplied the said drawings, specifications, or other data, is not to be regarded by implication or otherwise, or in any manner licensing the holder or any other person or corporation, or conveying any rights or permission to manufacture, use, or sell any patented invention that may in any way be related thereto.

Qualified users may obtain copies of this report from the Defense Technical Information Center.

References to named commercial products in this report are not to be considered in any sense as an indorsement of the product by the United States Air Force or the Government.

This report has been reviewed by the Office of Public Affairs (PA) and is releasable to the National Technical Information Service (NTIS). At NTIS, it will be available to the general public, including foreign nations.

APPROVAL STATEMENT

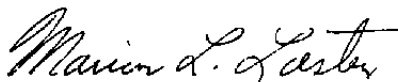
This report has been reviewed and approved.



MARSHALL K. KINGERY
Project Manager
Directorate of Technology

Approved for publication:

FOR THE COMMANDER



MARION L. LASTER
Director of Technology
Deputy for Operations

UNCLASSIFIED

REPORT DOCUMENTATION PAGE		READ INSTRUCTIONS BEFORE COMPLETING FORM
1 REPORT NUMBER AEDC-TR-79-97	2 GOVT ACCESSION NO.	3 RECIPIENT'S CATALOG NUMBER
4 TITLE (and Subtitle) ANALYSIS OF THE FLOW INTERACTIONS BETWEEN LARGE WATER DROPLETS AND AIR IN DROPLET ACCELERATION NOZZLES		5 TYPE OF REPORT & PERIOD COVERED Final Report-October 1978 to September 1979
7 AUTHOR(s) P. A. Kessel, ARO, Inc., a Sverdrup Corporation Company		6 PERFORMING ORG. REPORT NUMBER
9 PERFORMING ORGANIZATION NAME AND ADDRESS Arnold Engineering Development Center/DOT Air Force Systems Command Arnold Air Force Station, Tennessee 37389		8 CONTRACT OR GRANT NUMBER(s)
11 CONTROLLING OFFICE NAME AND ADDRESS Arnold Engineering Development Center/DOS Air Force Systems Command Arnold Air Force Station, Tennessee 37389		10 PROGRAM ELEMENT PROJECT TASK AREA & WORK UNIT NUMBERS Program Element 65807F
14 MONITORING AGENCY NAME & ADDRESS (if different from Controlling Office)		12 REPORT DATE May 1980
		13 NUMBER OF PAGES 43
		15 SECURITY CLASS (of this report) UNCLASSIFIED
		15a DECLASSIFICATION DOWNGRADING SCHEDULE N/A
16 DISTRIBUTION STATEMENT (of this Report) Approved for public release; distribution unlimited.		
17 DISTRIBUTION STATEMENT (of the abstract entered in Block 20, if different from Report)		
18 SUPPLEMENTARY NOTES Available in Defense Technical Information Center		
19 KEY WORDS (Continue on reverse side if necessary and identify by block number) drops jet streams mathematical predictions high velocity equations test facilities liquid jets acceleration gases two phase flow		
20 ABSTRACT (Continue on reverse side if necessary and identify by block number) The conditions under which large drops, on the order of 150 μ in diameter, are formed from high-velocity liquid jets and their subsequent behavior in high-velocity airstreams are discussed. The quasi-one-dimensional equations for fully coupled two-phase turbulent flow of a noncondensable gas with evaporating droplets in a convergent-divergent nozzle are formulated. Droplet performance predictions for the Dust Erosion Tunnel (DET) are		

UNCLASSIFIED

UNCLASSIFIED

20. ABSTRACT (Continued)

reviewed in the light of existing two-phase flow test data. Criteria for the aerodynamic design of a droplet acceleration nozzle that would inhibit droplet breakup are developed and used for studying the performance of a droplet acceleration nozzle in the AEDC High Enthalpy Arc Tunnel (HEAT) test facility (H-1) and the DET facility. The conclusion is that although acceleration of large drops without breakup is feasible, many problems will have to be solved to obtain high droplet velocities with large droplets.

PREFACE

The work reported herein was conducted by the Arnold Engineering Development Center (AEDC), Air Force Systems Command (AFSC). The results were obtained by ARO, Inc., AEDC Division (a Sverdrup Corporation Company), operating contractor for the AEDC, AFSC, Arnold Air Force Station, Tennessee. Mr. M. K. Kingery was the Air Force project manager. The work was done under ARO Project Nos. P35S-V5A and P35C-03B, and the manuscript was submitted for publication on November 20, 1979.

CONTENTS

	<u>Page</u>
1.0 INTRODUCTION	5
2.0 DROPLET BEHAVIOR	5
2.1 Droplet Formation	7
2.2 Droplet Breakup	10
2.3 Droplet Drag Coefficient	14
2.4 Droplet Evaporation	17
3.0 ANALYSIS OF DROPLET ACCELERATION	
3.1 Governing Equations	19
3.2 DET Predictions	23
4.0 DROPLET ACCELERATION NOZZLE OPTIMIZATION	
4.1 Criteria	27
4.2 Predictions	28
4.3 Droplet Injection	31
5.0 CONCLUDING REMARKS	33
REFERENCES	34

ILLUSTRATIONS

Figure

1. Observed Liquid Jet Breakup Regimes	7
2. Theoretical Water Droplet Velocity as a Function of Injector Pressure Drop	11
3. Predicted Maximum Droplet Diameter as a Function of Jet Injection Velocity	12
4. Observed Droplet Breakup Regimes	13
5. Drag Coefficient of Spheres and Drops, Ref. 16.	15
6. Calculated Droplet Diameter Decrease for DET	23
7. Predicted Droplet Behavior in DET Nozzle Throat	24
8. Effect of Droplet Mass Flow Rate and Drag Coefficient Increase Attributable to Droplet Distortion on Predicted Breakup Time for the DET Nozzle Throat Region	25
9. Effect of Droplet Injection Velocity on HEAT Optimized Droplet Acceleration Nozzle Performance	26

<u>Figure</u>	<u>Page</u>
10. Effect of Assumed Droplet Injection Velocity on the Design Point Performance of Droplet Acceleration Nozzles Optimized for the HEAT Facility	29
11. Effect of Assumed Critical Weber Number on the Design Point Performance of Droplet Acceleration Nozzles Optimized for the HEAT Facility	30
12. Droplet Acceleration Performance Predictions for Modified DET Nozzle	31
13. Droplet Injection Pressure Intensifier	32
14. Possible Droplet Injector/Arc Heater/Acceleration Nozzle Configuration	32

TABLE

1. DET and HEAT Facility Operating Parameters	6
---	---

APPENDIX

A. DERIVATION OF TWO-PHASE FLOW CONSERVATION EQUATIONS	37
NOMENCLATURE	40

1.0 INTRODUCTION

Natural water droplets and ice crystals in the atmosphere present a formidable hazard to ballistic vehicles during various phases of their trajectory. A number of studies have been made to determine the effect of ice crystals and water droplets on the performance of ballistic reentry vehicles (RV) (Refs. 1 and 2). The gun range has been used to determine the effect of snow and ice crystal impact on reentry vehicle nosetips for extremely short flight times (Ref. 3). At present, there is no facility that can simulate both the duration and intensity of the erosive environment induced by natural water droplets during the reentry phase of ballistic flight trajectories. The Arnold Engineering Development Center (AEDC) Dust Erosion Tunnel (DET) has been used successfully to simulate the environment created by atmospheric dust particles during the ascent phase of a ballistic vehicle's flight. In the AEDC High Enthalpy Arc Tunnel (HEAT) test facility (H-1)*, the kinetic energy flux on transpiration-cooled nosetips attributable to water droplet impacts has been simulated with graphite particles having a specific gravity of 1.7. Extending the simulation capability to include acceleration of water droplets would provide a more accurate simulation of the environment encountered by an RV nosetip in adverse weather during its ascent phase in the DET and its terminal phase in the HEAT facility. The survivability of droplets in these high-temperature facilities is, of course, the critical feasibility question.

In Fiscal Year 1977, an exploratory test was conducted by H. F. Lewis at AEDC in the DET in which liquid water (up to 15 percent of total mass flow) was injected through the existing particle injection system. The facility was operated at low enthalpy (600 Btu/lbm to encourage droplet survival. No particle diagnostics were installed to provide direct evidence of droplet survival; however, strong indirect evidence was obtained from stagnation point heat-transfer measurements which could be interpreted in terms of the latent heat of vaporization of droplets forming a heat sink at the model surface. In addition, some evidence of model surface erosion and/or accelerated chemical activity was observed. The current study was undertaken to determine whether droplet survival in the DET tests could be analytically verified and, more importantly, to determine whether appropriate modifications would produce a useful droplet erosive field in the DET and the HEAT facility.

2.0 DROPLET BEHAVIOR

This report is concerned with understanding and predicting the behavior of accelerating water droplets in supersonic nozzles at operating conditions usually associated with complete test model destruction. For a water droplet to survive such conditions, it must meet and overcome three specific hazards:

*The AEDC High Enthalpy Arc Tunnel (HEAT) test facility (H-1) is hereinafter referred to as the HEAT facility.

1. The droplet or its precursor must be injected into the nozzle in a manner consistent with the formation of the droplet and the basic flow process in the nozzle.
2. The droplet must resist breakup by the aerodynamic forces that produce its acceleration.
3. Enough of the initial droplet must survive evaporation to produce a meaningful test environment.

The design goal for a droplet acceleration nozzle is to accelerate water droplets of from 500- to 1,000- μ diameters to velocities that are associated with ascent and reentry trajectories. The operating parameters for the DET and HEAT are presented in Table 1.

Since there is no continuous water droplet acceleration facility presently available, attainment of even a fraction of the velocities indicated in Table 1 will be of some interest. It is expected, however, that droplet velocities will have to exceed 9,000 fps to be of lasting interest. Also, although droplet sizes of 500 μ are desired, more interest would result if smaller drops could be accelerated to high velocities.

Table 1. DET and HEAT Facility Operating Parameters.

	<u>DET</u>	<u>HEAT</u>
Throat Diameter (in.)	0.5625	0.375 to 0.700
Exit Diameter (in.)	4.36, 8.32, 15.34	0.850 to 1.600
Mach Number	5.9, 7.7, 9.5	1.8 to 3.5
P_o (atm)	20 to 68	20 to 120
h_{oB} (Btu/lmb)	400 to 1,800	400 to 4,000
P_e (atm)	0.044 to 0.0006	0.50 Min.
u_{gas} (fps)	4,300 to 9,200	2,800 to 11,100

2.1 DROPLET FORMATION

Since droplet formation has been of significant industrial importance for many years, there has been much research done concerning the breakup of liquid streams into drops. Although this study is restricted to the study of droplet injectors for the DET and HEAT nozzles, a short discussion of the full range of liquid jet breakup behavior will illuminate some of the problems inherent in droplet injector design.

In Ref. 4 and others, the jet breakup behavior is illustrated by showing a simplified model of an ideal, smooth, cylindrical injection tube discharging liquid into stagnant air at various liquid flow rates. The resulting flow patterns for an increasing liquid flow rate are illustrated in Figs. 1a through e.

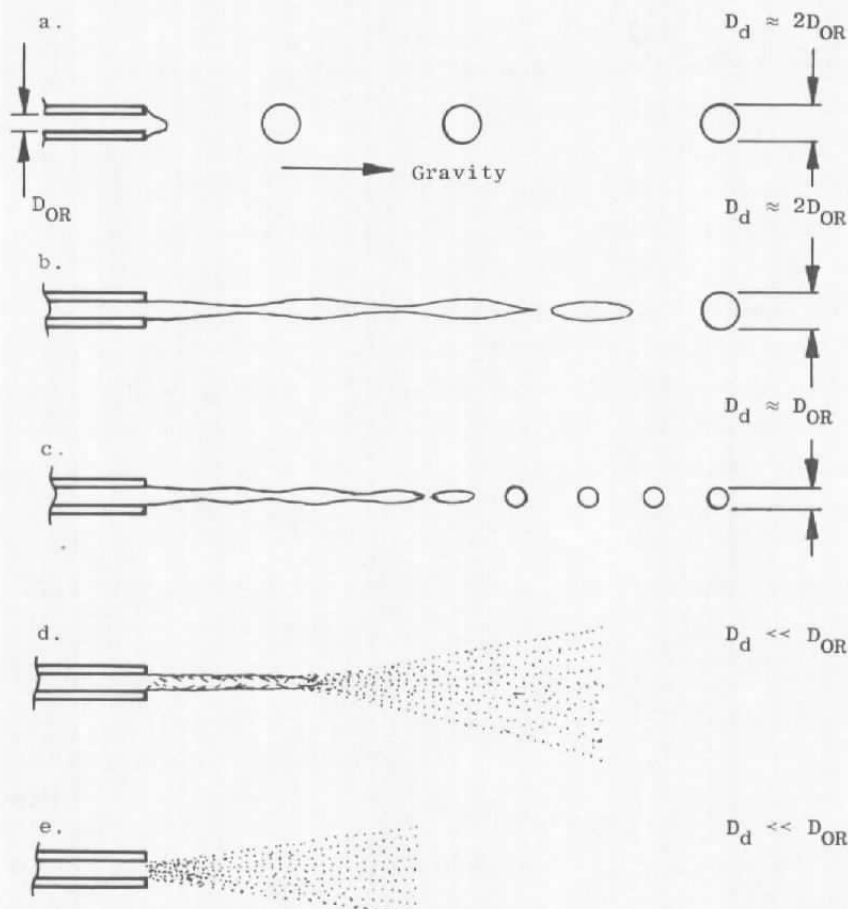


Figure 1. Observed liquid jet breakup regimes.

The flow pattern sketched in Fig. 1a represents a low flow regime in which the capillary forces completely dominate the flow. A drop remains attached to the injector until it is dislodged by the weight of the fluid, stray air currents, vibration, or some other force. The size of the drop is controlled by the liquid surface tension and injector geometry. Many experimenters have reported that the drop size is roughly twice the injector inside diameter.

In Fig. 1b, the liquid flow rate has been increased until a solid, clear, undisturbed jet is formed. The clarity of the jet is significant in that there are no surface waves on the jet surface; this implies that the aerodynamic forces are minimal. The jet surface oscillates because of the interaction between surface tension and inertial forces; these surface oscillations build to the point at which the jet is pinched off, forming long cylinders downstream of the injection point. These cylinders, in turn, form droplets that are approximately twice the jet diameter. This regime is called the Rayleigh regime and has been studied intensively.

At higher jet velocities, the aerodynamic forces induced by the motion of the jet become significant. The aerodynamic forces amplify and interact with the surface oscillations to increase their amplitude and produce jet breakup nearer the injector face, as is shown in Fig. 1c. The resulting droplets have the same diameter as the jet. This regime was called the "first wind-induced regime" by Weber, whose work is discussed in Refs. 5 and 6.

The second wind-induced regime, which occurs at even higher jet velocities, is characterized by a relatively short cylindrical jet that abruptly breaks up into small drops, producing a fan- or cone-like expansion, as shown in Fig. 1d. In this regime the surface aerodynamic forces are so much greater than the surface tension forces that the characteristic drop size, which is considerably smaller than the jet diameter, is only slightly dependent upon jet diameter.

The final regime, shown in Fig. 1e, is called the atomization regime because the jet is completely broken up into very small drops (i.e., atomized) at the injector exit. The jet has no cylindrical section and the cone-like expansion begins at the injector exit. Some experimental evidence suggests that the breakup process actually begins inside the injector and that it is associated with turbulence production in the injector.

Much empirical and analytical work has been done in attempts to describe the jet breakup in the atomization regime; important applications to such devices as paint sprayers and rocket propellant injectors have helped to prompt this work. There is a lack of analytical definition of the boundaries of the various breakup regimes, probably because the many secondary variables that affect the breakup process are uncontrolled, thus

complicating the precise definition of boundaries. The Rayleigh and first wind-induced breakup regimes are of primary importance to this study; it is unfortunate that the other, more stable, breakup regimes produce large quantities of very small droplets which tend to evaporate quickly in a nozzle.

The two critical questions of droplet behavior that must be answered are

1. Where does the liquid jet breakup occur?
2. What is the diameter of the resulting drops?

Calculation of a meaningful jet breakup time in either the DET or the HEAT facility is complicated by the fact that the injected jet is subjected to an extreme acoustic environment and a highly turbulent flow. Measurements of the environment inside the injector chamber have not been made, but pitot pressure measurements in the arc heater exit flow typically have fluctuations that are 2.5 percent of the mean value. The quantitative effect of the droplet injection chamber environment is also unknown. In view of the uncertain nature of the environment and its effect on the jet, the most conservative assumption to make is that the jet breaks up into droplets at the injector exit, although it could be possible that the jet could break up further downstream, producing larger droplets at the exit.

Many different droplet-size prediction models exist. The experimental work of Ingebo (Ref. 7) is similar to the earlier DET test in terms of type of injection, injection liquid, flow-field variables, and gas and liquid velocities, and is therefore most applicable to this study. Ingebo has correlated his results for accelerating water and ethanol drops in still and accelerating air, nitrogen, and helium streams as

$$\frac{D_{OR}}{D_{Max}} = 0.64 \left(\frac{D_{OR}}{D_t} \right)^{0.33} B_o^{0.33} Re_\ell^{-0.1} Re_g^{0.5} B_o^{-0.07} \times \left[0.044 + We_\ell We_g^{-0.2} B_o^{-0.07} \left(1.25 \times 10^{-6} + 0.33 \times 10^6 A_c^{0.5} B_o^{-0.67} \right) \right] \quad (1)$$

where

$$B_o = \text{Bond Number} = \frac{\rho_\ell D_{OR}^2 g}{\sigma_\ell} \quad (2)$$

$$We_x = \text{Weber Number} = \frac{\rho_x V_r^2 D_{OR}}{\sigma_\ell} \quad (3)$$

$$\Lambda_c = \text{Acceleration to surface tension ratio} = \frac{\rho_g D_{OR}^2 a}{\sigma_l} \quad (4)$$

The remaining terms and subscripts are explained in the Nomenclature.

The drop or jet velocity issuing from an injector can be predicted by

$$V = C_q \sqrt{\frac{2\delta_p}{\rho}} \quad (5)$$

where δ_p is the injector pressure drop and C_q is the empirical discharge coefficient, usually between 0.85 and 1.0.

A plot of Eq. (5) is shown in Fig. 2 for $C_q = 1.0$. It should be noted that in all of the literature searched concerning "high-speed jets," injector δ_p is limited to about 3,000 psi. No data and, hence, no correlations were found for what may be termed ultrahigh jet velocities on the order of 2,000 to 3,000 fps.

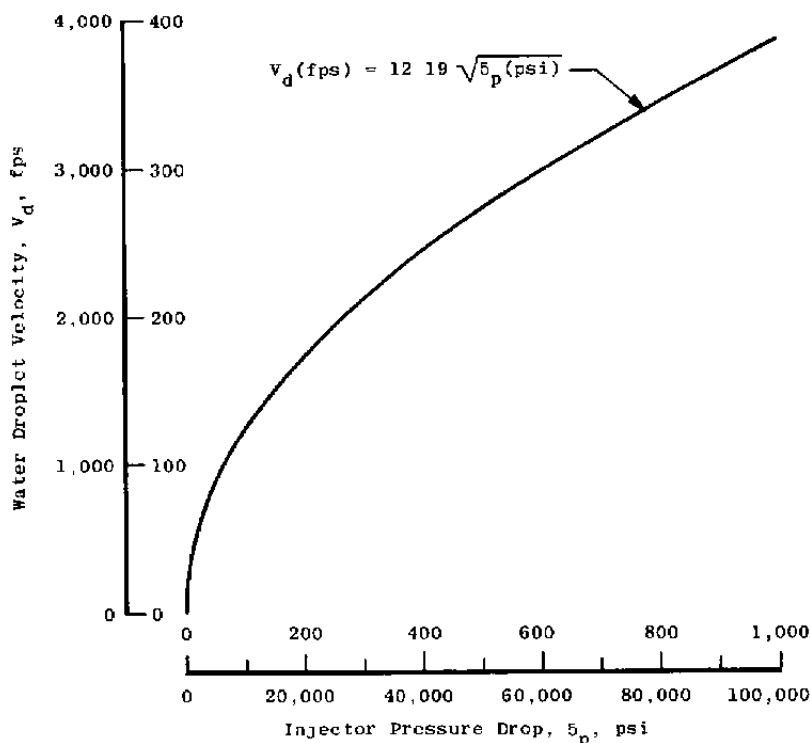


Figure 2. Theoretical water droplet velocity as a function of injector pressure drop.

Discussion of the practical problems associated with achieving high jet velocities will be deferred until Section 4.3, but it is appropriate to discuss the jet breakup problem here. Some investigators believe that atomization of the jet occurs because of the level of turbulence in the injector and not because of the jet velocity relative to the airstream. Figure 3 presents the maximum droplet diameter, D_{Max} , predicted by Eq. (I) as a function of the injection orifice diameter, D_{OR} , for two droplet injection chamber conditions.

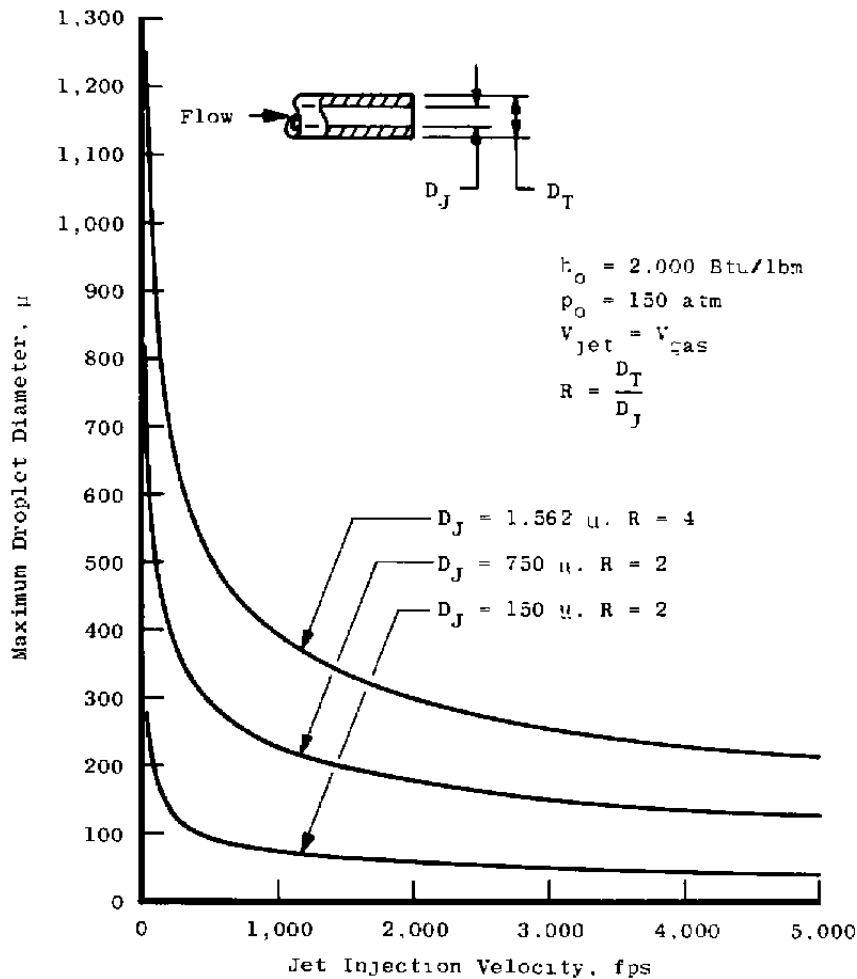


Figure 3. Predicted maximum droplet diameter as a function of jet injection velocity.

2.2 DROPLET BREAKUP

The most restrictive feature of the droplet behavior is the tendency for the droplet to deform and disintegrate when the aerodynamic loading exceeds a critical loading. The ratio

of droplet distorting aerodynamic forces to the droplet cohesive forces is defined as the Weber number:

$$We = \frac{\rho_g (u - V)^2 D_d}{\sigma_l} \quad (6)$$

A number of experimental studies of these phenomena have been made (Refs. 9, 10, and 11). The behavior of the drop as described in Ref. 4 is categorized by the five modes shown in Fig. 4.

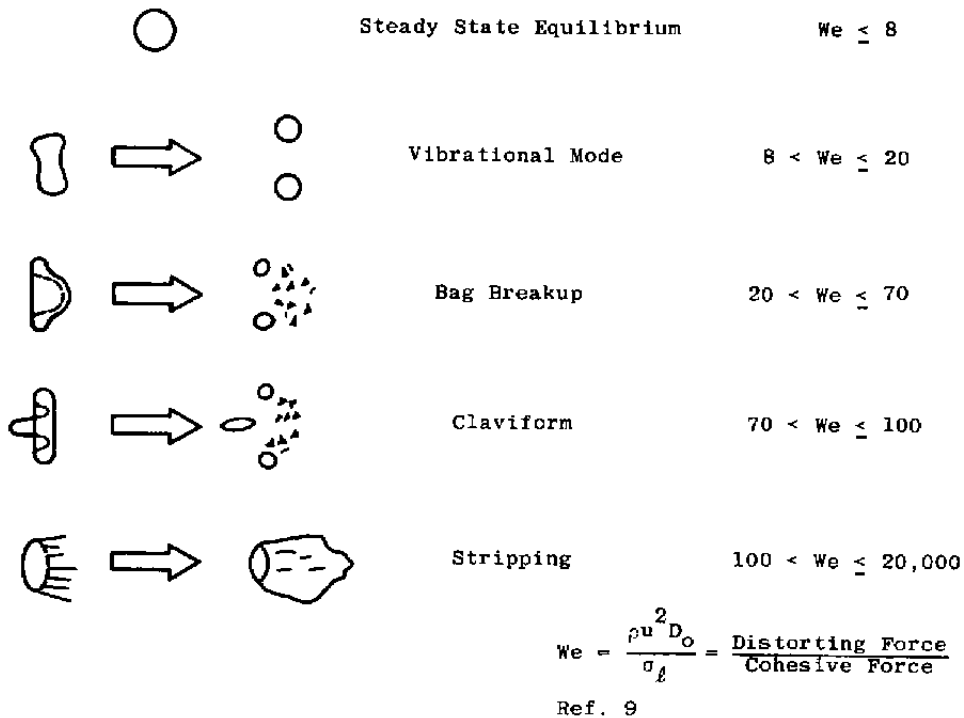


Figure 4. Observed droplet breakup regimes.

The critical Weber number is defined as the upper boundary of the first region, that of steady-state equilibrium. Values vary from 4 to 10 for the critical Weber number used in the studies. The value of 8, taken from Ref. 9, is used in the analytical portion of this study. Between the critical Weber number and a Weber number of 20, the droplet is observed to vibrate and eventually to break up into two or three equal-sized droplets. Between Weber numbers 20 and 70, the droplet deforms into a bag with a heavy rim before breakup. Between Weber numbers 70 and 100, the drop deforms as a bag plus a centerbody before

breakup. Between numbers 100 and 20,000, the drop flattens and the surface is blown (i.e., stripped) away. Above a Weber number of 20,000, the drop is said to enter the catastrophic mode of breakup in which it is torn apart virtually instantaneously. Two points should be apparent from Fig. 4: (1) Drops deform before breakup, and (2) droplet breakup is a transient process below a Weber number of 20,000.

Reinecke and Waldman performed a number of droplet experiments with a shock tube; they observed the behavior of droplets with flash x-ray and shadowgraph devices. They correlated (Ref. 9) the time required for a droplet to break up after passing through a normal shock wave as

$$\begin{aligned}
 T_b &= \frac{22(W_e - 8)^{-1/4}}{Q_{Max}^{1/2}} \quad \text{For } 8 < W_e \leq 1,700 \\
 T_b &= \frac{0.013(W_e - 8)^{3/4}}{Q_{Max}} \quad \text{For } 1,700 < W_e \leq 2,700 \\
 T_b &= \frac{35.0(W_e - 8)^{-1/4}}{Q_{Max}^{1/2}} \quad \text{For } 7,700 < W_e
 \end{aligned} \tag{7}$$

where

$$Q_{Max} = \frac{q_{Max \text{ on Drop}}}{q_\infty} \approx 0.78 + \frac{1.47}{1.0 + 2.1 M_r^{3.4}} \tag{8}$$

$$T_b = \frac{t_b V_r \rho_g}{D_{c1} \rho_l} \tag{9}$$

In these experiments the flow behind the shock is steady, and the droplet is accelerating toward equilibrium with the flow. In the droplet acceleration nozzles under study here, both the droplet and the gas are accelerating. Equations (6), (7), and (8) are used as the transient droplet breakup criteria by requiring that

$$\int_0^t \frac{dT_b}{T_b} = 1 \tag{10}$$

before the droplet can be said to have disintegrated.

The droplet dilation ratio observed in Ref. 9 can be summarized as follows:

$$\frac{D_d}{D_{d1}} = 1 + 1.5T^2 \quad 1.75 \text{ Max. observed} \quad \text{For } 0 \leq W_e < 2,000 \quad (11)$$

$$\frac{D_d}{D_{d1}} = 1 + 2.2T \quad 4.8 \text{ Max. observed } 0 < T < 1.8 \quad \text{For } 2,000 \leq W_e < 3,200 \quad (12)$$

$$\frac{D_d}{D_{d1}} = 1.203T \quad 3.5 \text{ Max. observed} \quad \text{For } 3,200 \leq W_e \quad (13)$$

The dilation behavior in the intermediate Weber number region was odd, and the scatter in all regions was large. The relations

$$\frac{D_d}{D_{d1}} = 1 + 1.5T^2 \quad (14)$$

$$\left(\frac{D_d}{D_{d1}} \right)_{\text{Max}} \approx 2.5 \quad (15)$$

are used in the study for all Weber numbers.

2.3 DROPLET DRAG COEFFICIENT

According to Ref. 12, the net force on a droplet is comprised of several components:

$$F = F_\tau + F_p + F - F_{Ba} + F_{am} + F_{Body} \quad (16)$$

where

- F_τ = Viscous shear forces
- F_p = Surface pressure forces
- F_{am} = Force attributable to mass entrained in droplet boundary layer
- F_{Ba} = Bassett force attributable to unsteady motion of flow around the droplet

$$F_{\text{body}} = \text{Body force attributable to gravity and to electrostatic and magnetic fields.}$$

The forces attributable to gravity, electromagnetic fields, apparent mass, and unsteady fluid motion can be shown to be small for droplet and nozzle flow conditions under consideration. [See Soo (Ref. 12) and Rudinger (Ref. 13) for details.]

The electrostatic forces can also be neglected in this study, but under some conditions, the electrostatic force either advertently or inadvertently applied can be significant (Ref. 14). The remaining forces are grouped together and are described by the droplet drag coefficient to which appropriate corrections are made to account for the effects of nozzle pressure gradient and droplet volume fraction.

Comparison of droplet drag coefficient measurements is complicated by the tendency of the droplets' surfaces to distort, slip, and vaporize. A comparison of various data to the standard incompressible sphere drag curve is shown in Fig. 5, taken from Ref. 15. The data of Hughes and Gilliland (Ref. 16) are for freely falling drops of various diameters. The data of Ingebo (Ref. 17) are for accelerating droplets of various liquids. The disagreement or scatter of these data (i.e., from 0.2 to 1.0), at Reynolds numbers between 400 and 500 indicates that droplet calculations in this range are approximate at best.

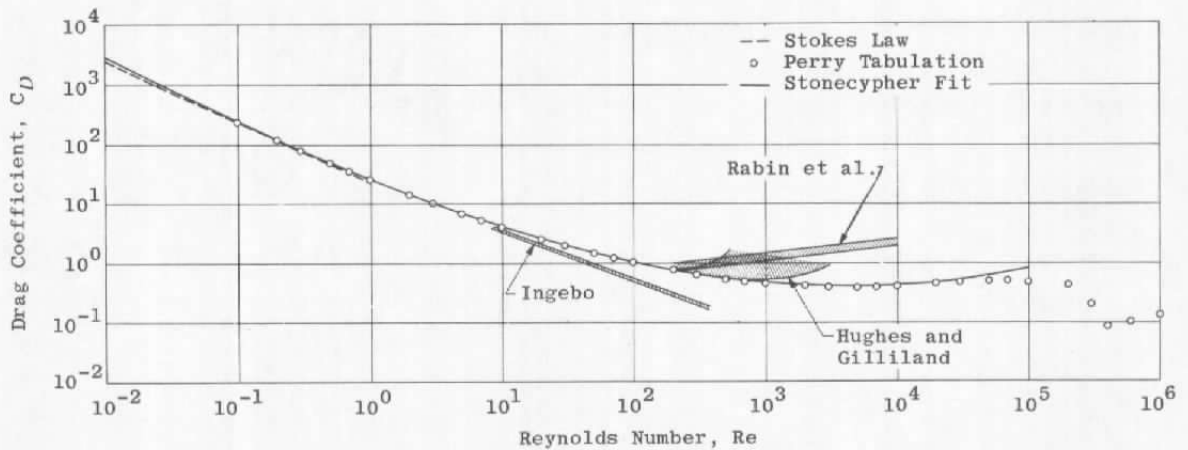


Figure 5. Drag coefficient of spheres and drops, Ref. 16.

The curve fit to a standard drag curve presented in Ref. 15

$$C_d = \frac{24}{Re_d} \quad \text{For } Re_d \leq 0.01 \quad (17)$$

$$C_d = \exp \left[3.271 - 0.8893 (\ln Re_d) + 0.03117 (\ln Re_d)^2 + 0.001443 (\ln Re_d)^3 \right] \quad \text{For } 0.1 < Re_d \leq 20,000 \quad (18)$$

$$C_d = 0.4569 \quad \text{For } Re_d > 20,000 \quad (19)$$

is used in this study with appropriate correction factors. When one derives optimum nozzle contours, the use of a single relationship for drag coefficient between $Re_d = 0.01$ and $Re_d = 20,000$ precludes any problems attributable to drag curve mismatch. Mach number correction to the standard drag curve is not necessary since the relative Mach number of viable drops will be low in areas in which small changes in the drag coefficient are significant.

The nominal value of droplet C_d must be increased if the droplet spacing approaches a value of several droplet diameters. Tam (Ref. 18) estimates that the drag coefficient of a sphere in incompressible flow will be multiplied by a factor as follows:

$$\frac{C_d}{C_{d_{\text{Stokes}}}} = \frac{4 + 3\epsilon + 3(8\epsilon - 3\epsilon^2)^{1/2}}{(2 - 3\epsilon)^2} \quad (20)$$

where ϵ is the fraction of space occupied by the particle volume. The liquid volume fraction is less than 0.2 percent for the conditions considered in the study; consequently, it is not necessary to make the drag coefficient correction indicated by Eq. (20).

However, an additional correction is required to account for the effect of the nozzle pressure gradient. Since the force on a droplet attributable to pressure gradient is

$$F_g = Vol_d \frac{dp}{dx} \quad (21)$$

then

$$\delta C_d = \frac{Vol_d \frac{dp}{dx}}{A_d q} = \frac{2D_d \frac{dp}{dx}}{3 q} \quad (22)$$

This correction is usually neglected; however, the small throat diameter and radius of curvature and the high reservoir pressure of the DET and HEAT facility nozzles create an unusually large pressure gradient that can increase the droplet drag coefficient by 100 percent. Because of the nature of this force (i.e., its similarity to the buoyant force which accelerates vapor bubbles), it probably does not increase the distortion of the droplet and, hence, is highly advantageous. Paradoxically, contouring the nozzle to produce a gradual droplet acceleration, inhibiting droplet breakup by aerodynamic forces, reduces this favorable force to an insignificant level.

2.4 DROPLET EVAPORATION

In general, accurate computation of droplet evaporation requires full consideration of heat and mass transfer through the binary boundary layer of the evaporating drop. The parameters that best describe this process are the Nusselt number (Nu) and the diffusion Nusselt number (Nu'). These parameters have been correlated by many investigators who agree with Ref. 19 that

$$Nu = 2.0 + 0.60 Re^{1/2} Pr^{1/3} \quad (23)$$

and

$$Nu' = 2.0 + 0.60 Re^{1/2} Sc^{1/3} \quad (24)$$

where

$$Nu = \frac{D_d h_f}{k_m} \quad (25)$$

and

$$Nu' = D_d \frac{\bar{R}_u T_m}{M_v} \frac{K_g}{D_{ab}} \quad (26)$$

It should be noted here that Eqs. (23) through (26) reflect the value of the Nusselt numbers observed in many different tests and, as such, cannot predict the effects of some aspects of the flow that are unique to the arc jet facilities, such as free-stream turbulence. The heat-transfer and mass-transfer rates to the drop may be calculated from

$$\dot{q} = h_f(T_g - T_{ds}) = k_\ell \frac{\partial T}{\partial r} + \frac{\dot{m}}{S_d} \left[\lambda + C_{p_v}(T_g - T_{ds}) \right] \quad (27)$$

and

$$\frac{\dot{m}}{S_d} = K_g p \ell_n \frac{p - p_{v_\infty}}{p - p_{v_s}} \quad (28)$$

Equations (27) and (28) are also taken from Ref. 19, although Eq. (28) has been modified by the inclusion of the vapor pressure of the surrounding gas flow, p_{v_∞} . The mass flow in Eq. (27) is the rate at which the droplet loses mass, whereas the mass flow in Eq. (28) is the rate at which the droplet mass is passed through the droplet's boundary layer by diffusion. These rates may be equated under most conditions. The energy balance of Eq. (27) includes a droplet radial heat conduction term, $K_\ell (\partial T / \partial r)$. This usually insignificant term plays an important role in the change of phase of a drop when there is no heat transfer or diffusion through the drop's boundary layer, such as when a drop is in both velocity and thermal equilibrium with a gas whose pressure is decreased to a level below the equilibrium saturation pressure. In such a case, the droplet conditions necessary for evaporation (i.e., nonequilibrium), are created as the pressure wave associated with the pressure change passes through the drop. Evaporation or boiling first occurs at a nucleation site or phase boundary as the driving potential is increased. In this case, the evaporation occurs immediately at the drop's surface without any accompanying mass diffusion through the boundary layer. The evaporation is limited only by the rate at which the latent heat of vaporization can be supplied by conduction from the interior of the drop. That is, Eq. (26) degenerates to

$$\frac{\dot{m}}{S_d} = - \frac{k_\ell}{\lambda} \frac{\partial T}{\partial r} \quad (28)$$

Very large rates of droplet temperature change are generated by seemingly insignificant droplet temperature gradients for small drops. For example, the temperature-time derivative for a 25- μ drop with a 1°R linear temperature differential between the surface and the center of the drop is

$$\begin{aligned} \frac{\partial T}{\partial t} &= \frac{6 k_\ell}{C_{p_\ell} \rho_\ell D_d} \frac{\partial T}{\partial r} \\ \frac{\partial T}{\partial t} &= 2,756 \text{ } ^\circ\text{R/sec} \end{aligned} \quad (29)$$

In such cases it is plausible to assume that a state of equilibrium exists. This assumption removes the need for the radial conduction term in the droplet energy equation [Eq. (27)]

which is required only for this case. The assumption can be used to delete the diffusion equation [Eq. (27)] and replace it with the specification of droplet surface pressure:

$$p_{vs} = p, \text{ which implies } T_{ds} = T_{vs} = f(p) \quad (30)$$

where f is the relationship of vapor temperature to vapor pressure, with which the droplet energy equation can be solved for the evaporation rate as a function of pressure and heat-transfer rate.

3.0 ANALYSIS OF DROPLET ACCELERATION

A review of the earlier DET test data indicated that a droplet erosive field might be obtained in the DET; however, subsequent analysis using the one-dimensional particle acceleration nozzle program of Ref. 8, which was modified to calculate droplet evaporation and breakup, did not support this contention. Further review of the test data and the describing equations indicated that including the momentum and energy coupling term between droplet phase and nozzle gas phase would improve the analysis.

3.1 GOVERNING EQUATIONS

The one-dimensional channel flow of a noncondensable gas with concurrent flow of a liquid and its vapor can be described by three global conservation equations, two coupling relations for the gaseous and liquid phases momentum and energy, an equation describing the rate of phase change, and three equations of state. Auxiliary relations are required to determine the global equation of state in terms of the component parts and the gas phase transport properties in terms of the noncondensable gas properties, the vapor properties, and the vapor fraction, \dot{m}_d/\dot{m}_g . The equations to be integrated are as follows:

Conservation of Global Mass [Eq. (A-2)]

$$\frac{1}{u} \frac{du}{dx} - \frac{1}{h} \frac{dh}{dx} + \frac{2}{D_N} \frac{dD_N}{dx} + \frac{1}{p} \frac{dp}{dx} - \frac{1}{R} \frac{dR}{dx} = - \frac{3}{D_d} \frac{\dot{m}_d}{\dot{m}_g} \frac{dD_d}{dx} \quad (31)$$

Conservation of Global Momentum [Eq. (A-4)]

$$\frac{du}{dx} + \frac{A_N}{\dot{m}_g} \frac{dp}{dx} + \frac{\dot{m}_d}{\dot{m}_g} \frac{dV_d}{dx} - \frac{3}{\dot{m}_g} \frac{\dot{m}_d}{D_d} \frac{(u - V_d)}{dx} \frac{dD_d}{dx} = - \frac{2u C_f}{D_N} \quad (32)$$

Conservation of Energy [Eq. (A-5)]

$$u \frac{du}{dx} + \frac{dh}{dx} + \frac{\dot{m}_d}{\dot{m}_g} \left(V_d \frac{dV_d}{dx} + C_{p_d} \frac{dT_d}{dx} \right) + \frac{3}{\dot{m}_g} \frac{1}{D_d} \frac{dD_d}{dx} \left(C_{p_d} T_d + \frac{V_d^2}{2} - h - \frac{u^2}{2} \right) = - \frac{4C_h}{D_N} (h_o - h_w) \quad (33)$$

Particle Velocity (from Newton's Second Law, applied to a drop) [Eq. (15) of Ref. 19]

$$\frac{dV_d}{dx} = \frac{3}{4} \frac{C_d \rho(u - V_d) |u - V_d|}{D_d V_d \rho_d} \quad (34)$$

Particle Temperature (from a balance of aerodynamic heat transfer, internal energy of a droplet, and the latent heat and sensible heat of an evaporating fraction of the drop) [Eq. (37) of Ref. 15]

$$\frac{dT_d}{dx} = \left(\frac{Q_d}{m_d V_d} - \frac{dm_d}{dx} \frac{\delta h_d}{m_d} \right) \frac{1}{C_{p_d}} \quad (35)$$

where

$$Q_d = \pi D_d Nu C_{p_g} \mu (T_{o_d} - T_\ell) = \text{Rate of Heat Transfer to a Drop} \quad (36)$$

$$\delta h_d = \lambda + C_{p_d} (T_{vap} - T_d) + C_{p_v} (T_{o_d} - T_{vap}) \quad (37)$$

and

$$\frac{dm_d}{dx} = \frac{-\pi D_d^2 K_g p}{V_d} \ln \left(\frac{p - p_{vap}}{p - p_{vap\infty}} \right) \quad (38)$$

The term $(1/v) (d\bar{R}/dx)$ is evaluated numerically from the previous calculation. This vanishes for ideal-gas calculations.

The integration of the equations is accomplished by estimating the downstream pressure and, hence, the pressure gradient required to obtain some desired downstream condition, such as in matching the flow diameter to fit the nozzle contour:

$$\frac{1}{A_N} \frac{dA_N}{dx} = \frac{2}{D_N} \frac{dD_N}{dx} = \frac{4}{D_N} \tan \phi \quad (39)$$

$$\frac{dp}{dx} = \frac{\rho u^2}{1 - M^2} \frac{1}{A_N} \frac{dA_N}{dx} \quad (40)$$

Equation (39) is derived from isentropic flow theory. This equation is used successfully to predict the value of dp/dx for nonisentropic flow because, in practice, the δA term includes the correction for any previous errors and simplifying assumptions as well as for the change in true nozzle area in the interval δX .

This equation represents a change from the procedure used in Ref. 8 and has two distinct advantages:

1. In Eq. (40) the problem of dealing with the implicit sonic flow singularity in the system of ordinary differential equations is replaced with the problem of dealing with an explicit singularity whose behavior can be monitored. As a practical matter, limiting the pressure gradient to small negative values in the region near Mach 1 eliminates the mathematical problem. The gas-dynamic problem of matching the sonic point to the throat is handled, as always, by iterating on inlet mass flow for constant inlet total pressure and total enthalpy.
2. Equation (37) can be replaced with other algebraic equations to optimize the nozzle contour for any conceivable criteria. (See Section 4.1 for specific details).

The skin-friction coefficient for a smooth-walled pipe is given by the relation

$$C_f = 0.0014 + 0.125 \times Re^{-0.32} \quad (41)$$

taken from Ref. 26. The nozzle wall heat-transfer rate is calculated with use of Reynolds' analogy between heat and momentum transport as

$$C_h = 0.53 C_f \quad (42)$$

The equation of state for air

$$\rho = \rho(p, h) \quad (43)$$

is determined from curve fits to the data of Brahinsky and Neel (Ref. 20). Similarly, the equation of state of water vapor

$$\rho_{vap} = \rho(p, T) \quad (44)$$

and the definition of the liquid-vapor interface

$$T_{vap} = T(p) \quad (45)$$

$$P_{vap} = p(T) \quad (46)$$

$$h_{\ell_{vap}} = h(p) \quad (47)$$

are determined by curve fits to the data of Ref. 21. The surface tension of liquid water in air

$$\sigma = \sigma(T) \quad (48)$$

is determined from curve fits to the data of Refs. 23, 24, and 25. The diffusion coefficient for water vapor in air

$$D_{ab} = D_{ab}(T_{max}, p) \quad (49)$$

was determined from the data of Ref. 23.

Equations (31) through (49) are written in terms of the average gas and particle properties and, as a result, are as accurate as the values of C_f , C_h , and C_d used. With this one limitation, there is no reason why this solution should not be applicable to calculations beyond the merge point of the turbulent boundary layer of long slender nozzles. The previous analysis, presented in Ref. 8, used a friction coefficient (C_f) that was calculated with the implicit assumption that the boundary layer was not merged; hence, this analysis was optimistic. The present analysis does not make this assumption; however, in recognition of the fact that the centerline values of the flow variables are different from the average values, the centerline flow conditions are estimated with the assumption that isentropic flow exists between the nozzle inlet and the nozzle exit along the nozzle centerline. These calculations are made to determine to what extent the nozzle centerline conditions differ from the average conditions. The resulting centerline calculations are accurate up to the merge point. The centerline calculations beyond the boundary-layer merge point represent a theoretical limit that cannot be reached.

3.2 DUST EROSION TUNNEL PREDICTIONS

The equations described in Section 3.1 were programmed for an IBM 370/150 computer and were used to predict the droplet trajectories in the DET nozzle for the conditions of the earlier test:

$$p_o = 506 \text{ psia}$$

$$h_o = 487 \text{ Btu/lbm}$$

$$\dot{m}_{H_2O} = 0.347 \text{ lbm/sec}$$

The results of the analysis suggest that small droplets could have survived in the DET nozzle if the droplet model described in Section 2.0 is accurate. The calculations of droplet evaporation predict that all droplets having an initial diameter (D_i) greater than 10μ will survive evaporation, as shown in Fig. 6. Conversely, the calculations of droplet breakup based on the approximate model of Section 2.2 predict that droplets with an initial diameter of 15μ will exceed a Weber number of 8 and, hence, begin to break up 0.60 in. upstream of the DET throat, as shown in Fig. 7; the droplets will have completed the breakup process at

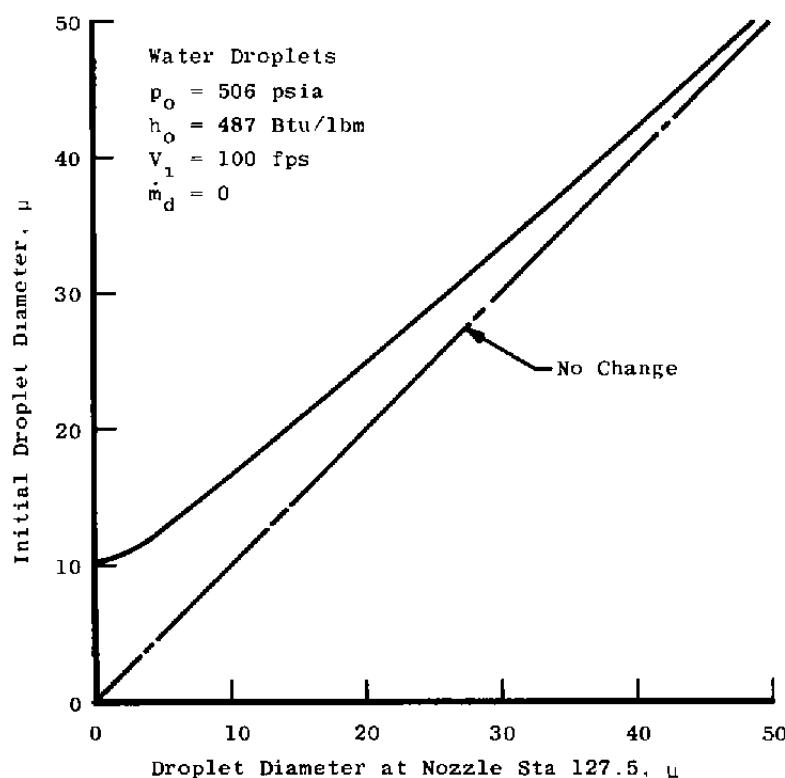


Figure 6. Calculated droplet diameter decrease for DET.

0.15 in. upstream of the throat, as shown in Fig. 8. The entire breakup process occurs in 0.45 in. of droplet travel, or approximately 762 initial, droplet diameters. Breakup time calculations are not presented for droplets having initial diameters of $10\ \mu$; however, it can be inferred by linear extrapolation of the peak Weber numbers (see Fig. 7) that droplets with initial diameters greater than $10\ \mu$ and somewhat less than $15\ \mu$ would probably have survived the breakup process and, hence, would produce droplets smaller than $8.0\ \mu$ in the DET test section.

Further calculations could be made to determine the precise initial diameter (between 10 and $15\ \mu$) of the largest droplet that could survive the breakup process described in Section 2.2, if such droplets were of anything but academic interest. A more profitable pursuit is suggested by the Weber number plot of Fig. 7, which shows that the droplet breakup conditions occur only in the nozzle throat. Thus, droplet breakup might be prevented if the throat is recontoured to limit droplet acceleration to some low value (i.e., to a Weber number less than 8.0).

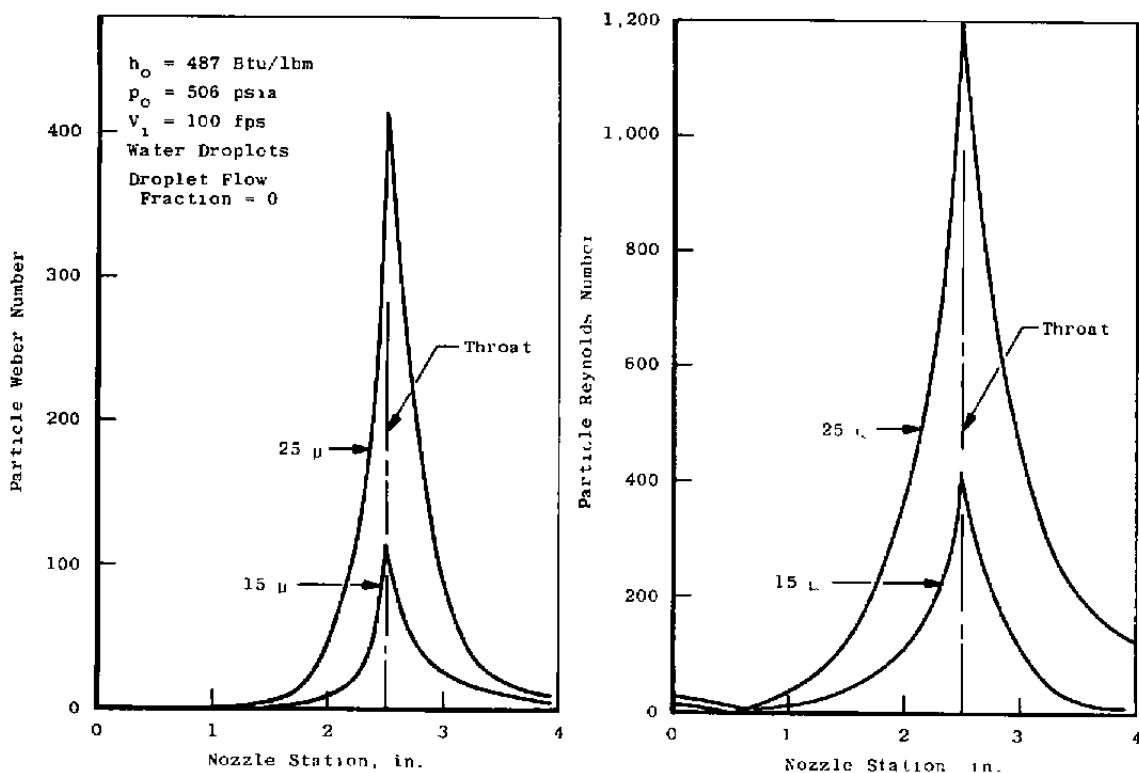


Figure 7. Predicted droplet behavior in DET nozzle throat.

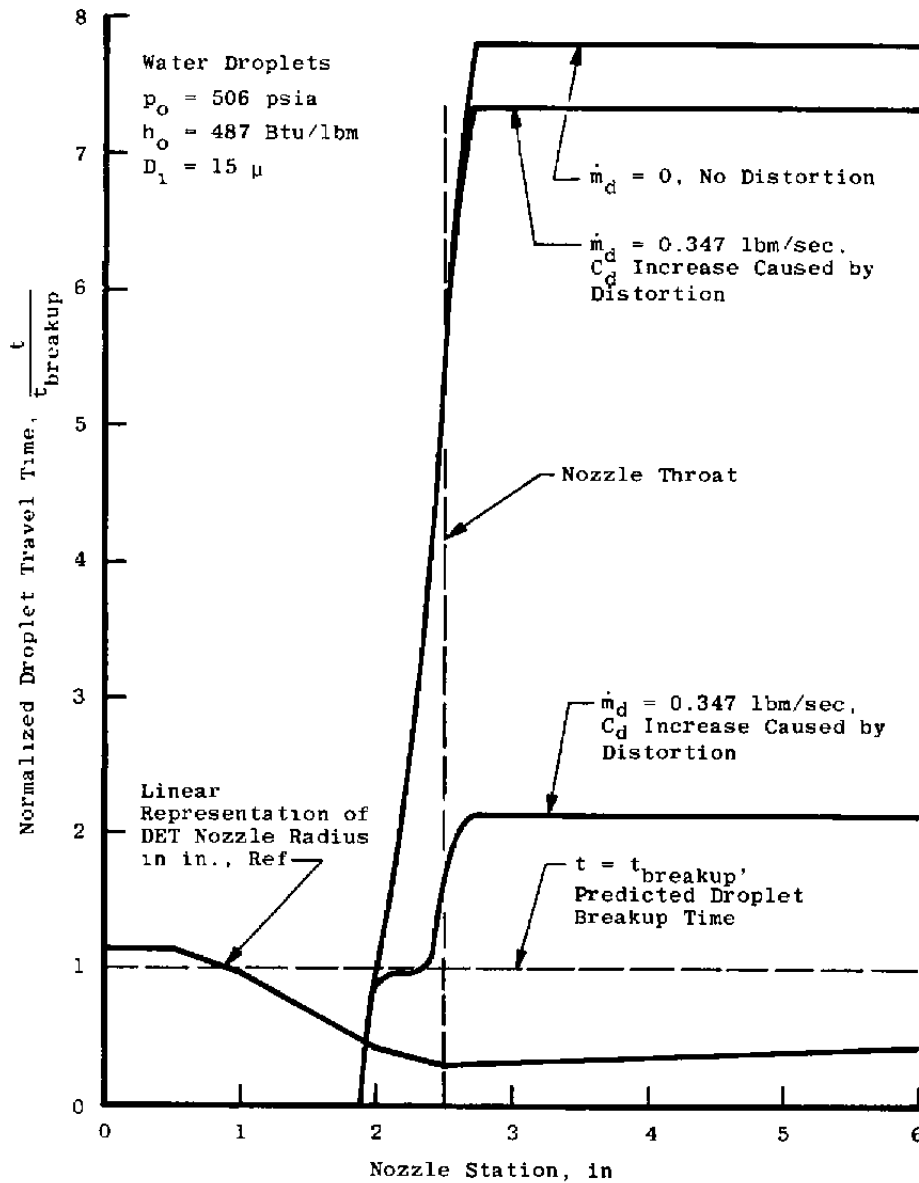


Figure 8. Effect of droplet mass flow rate and drag coefficient increase due to droplet distortion on predicted breakup time for the DET nozzle throat region.

4.0 DROPLET ACCELERATION NOZZLE CONTOUR OPTIMIZATION

The object of the optimization process discussed here is to limit the droplet Weber number to a value below which droplet breakup will not occur. A value of 8 has been chosen tentatively for this study; other purposes would have produced other "optimum" results. Narkis and Gal-Or (Ref. 27) defined the contour necessary to limit the evaporation of drops in two-phase flow and, with a similar analysis, came to some strikingly different conclusions, which were correct for their purposes. In their complete analysis, Elliot and Weinberg (Ref. 15) defined a nozzle contour necessary to maximize the exit velocity of constant-diameter water drops. Other analyses of optimization criteria for two-phase flow systems may be found in Refs. 15, 27, and 28.

The salient feature of the present analysis is that it entails a simple modification of an existing accurate predictive code that treats the fully coupled conservative equations for two-phase flow of an equilibrium real-gas and water vapor at high pressures and moderate enthalpy, including wall friction and heat transfer.

4.1 OPTIMIZATION CRITERION

The basic optimization criterion used in this study—limiting the Weber number to an arbitrary value—follows directly from the conclusions reached in Section 3.0: that low values of Weber number associated with small, initial, drop diameters reduce the final droplet size through increased evaporation and that high values of Weber number result in droplet breakup. The optimization process is involved at every step in the marching solution of the system of ordinary differential equations of Section 3.1; the process is used to determine the downstream pressure required to produce a Weber number of the desired limiting value.

With the assumptions that constant total enthalpy and total pressure exist in the gas phase and that constant surface tension exists for the predicted step, the downstream pressure is calculated from the following functional dependence:

$$p_2 = f\left(p, D_x, We, We_c, M_1, u_1, h_1, \rho_1, V_{d1}, D_1, D_{d1}, \frac{\partial D_d}{\partial x}, \frac{\partial V_d}{\partial x}\right) \quad (50)$$

This functional dependence [Eq. (50)] is an approximation, but it works extremely well in regions of low pressure gradient. The resulting value of Weber number, in areas of high pressure gradient, is as much as 2.5 percent low, which is consistent with the approximate value of the critical Weber number. Two more fundamental problems occur at the nozzle inlet and exit. At the nozzle inlet or, more precisely, at the droplet injection plane, the

optimization criterion demands an immediate and unrealistic change in nozzle area. This is circumvented by using the droplet injection conditions and the critical Weber number to determine the starting conditions for the optimization process. A similar problem occurs near the exit of high Mach number nozzles, where the gas density falls so low that the local Weber number is much less than the critical Weber number. In these cases, the optimization process is no longer necessary, and the nozzle contour should be specified by some other criterion. For the conditions of this study, it was found that the droplet velocity cannot be appreciably increased past the point at which the droplet critical Weber number is not a problem.

4.2 DROPLET ACCELERATION NOZZLE PERFORMANCE PREDICTIONS

A limited parametric study of the factors affecting droplet acceleration nozzle performance was made for a HEAT facility and a few limited calculations were made for the DET. The HEAT facility nozzle received more attention since the characteristically lower expansion ratio in that facility allows faster, more economical calculations that retain all of the important characteristics of the processes common to both facilities, except for droplet freezing that can be predicted only by DET solutions.

Preliminary calculations indicated that droplets injected at velocities compatible with the existing particle injection systems in the DET and the HEAT would probably not survive to the exit of the optimized nozzles at even moderate reservoir enthalpy levels. This is further aggravated by the fact that droplet and gas velocities vary with the square of the reservoir enthalpy.

One possible solution to this problem is to increase the droplet injection velocity to minimize the droplet mass loss in the subsonic section of the nozzle. As a practical concern, the maximum droplet injection velocity is severely limited by the available droplet injection pressure as is shown by Fig. 2. The predicted effect of droplet injection velocity is shown in Fig. 9. As expected, the exit droplet diameter increases almost linearly with increase in injection velocity from $13\ \mu$ at 600 fps to $30\ \mu$ at 3,000 fps for an initial, droplet diameter of $50\ \mu$. It is unfortunate that these larger drops require very long acceleration times, which involve long nozzle lengths and large reductions in exit bulk enthalpy because of wall heat transfer. The exit droplet velocity is 4,900 fps for an injection velocity of 3,000 ft/sec, which represents an increase of only 1,900 fps. Increasing the injected drop size from 50 to $150\ \mu$ decreases the exit velocity from 5,700 to 3,200 fps (as shown in Fig. 10) for injection velocity of 600 fps. Figure 10 also shows that the predominant effect of high injection velocity is to increase the exit drop diameter. The exit bulk enthalpy again decreases as the drop size

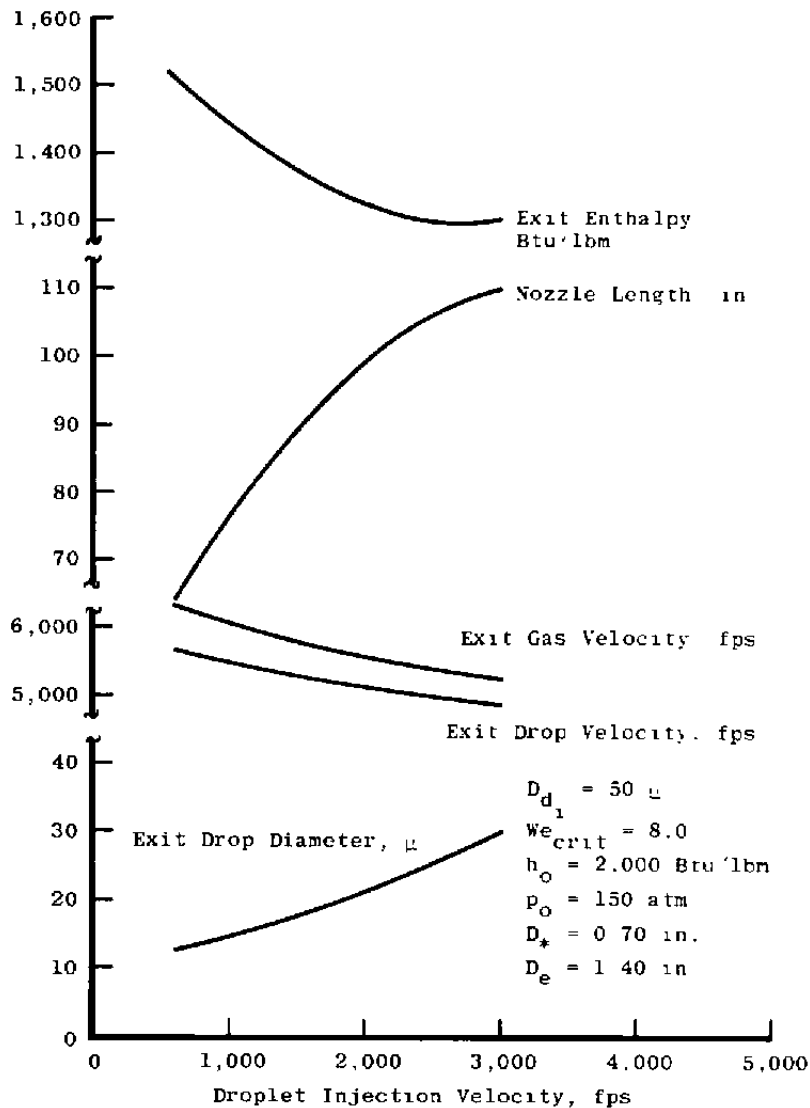


Figure 9. Effect of droplet injection velocity on HEAT optimized droplet acceleration nozzle performance.

increases. The performance of the droplet acceleration nozzle for the $150\text{-}\mu$, 3,000-fps point is poor since viturally half the bulk enthalpy is lost through the nozzle walls. The droplet breakup criterion severely limits acceleration of large droplets.

Performance could be improved considerably if the droplet breakup could be inhibited in some manner, such as by increasing the surface tension. This is shown in Fig. 11, in which the droplet breakup Weber number is assumed to be as high as 24. The increased breakup Weber number increases the droplet exit diameter and exit enthalpy. The performance of the DET nozzle with a 5,000-psi droplet injection system is shown in Fig. 12.

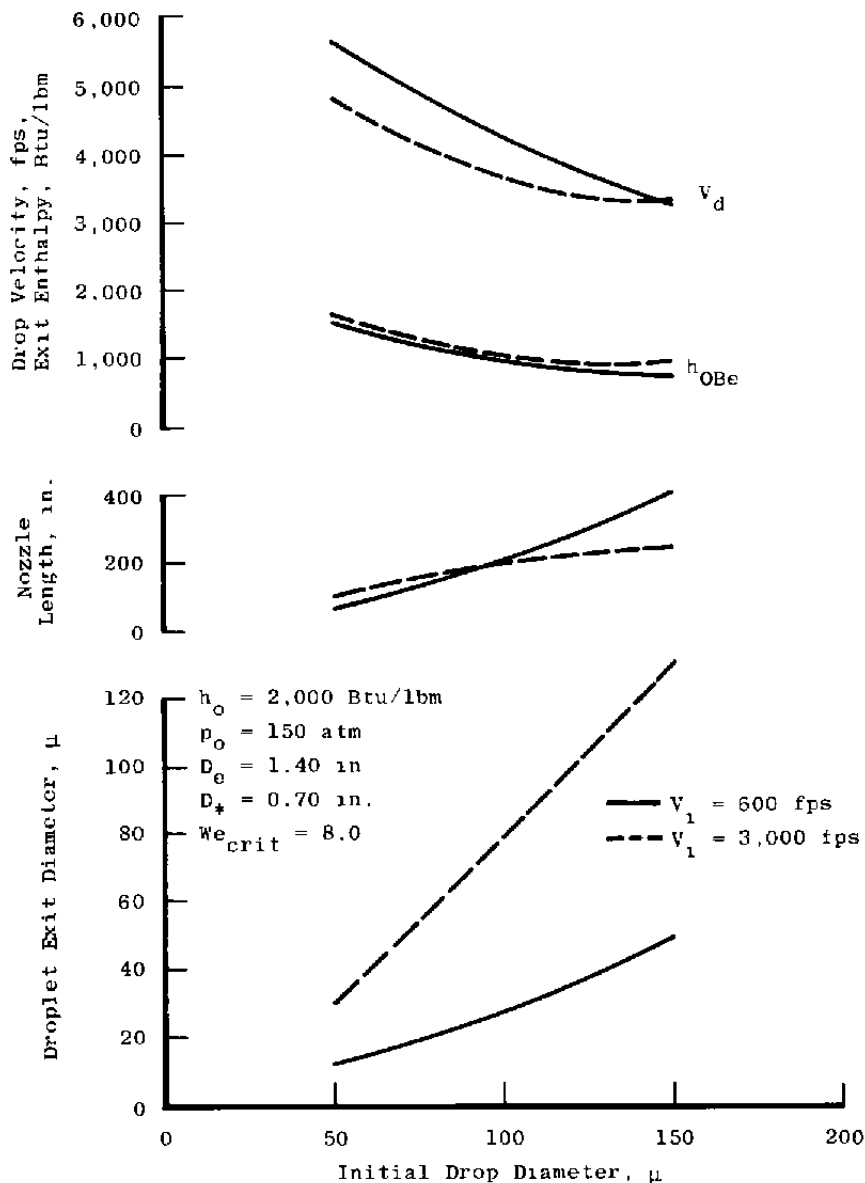


Figure 10. Effect of assumed droplet injection velocity on the design point performance of droplet acceleration nozzles optimized for the HEAT facility.

The 5,000-psi injection system produces theoretical droplet injection velocity of 770 fps. The predicted droplet exit velocity is rather insensitive to droplet injection diameter, varying only slightly between 4,700 and 4,800 fps.

Further study is needed to determine the full impact of varying the other system variables such as throat diameter and nozzle pressure; however, one problem that so far seems

inherent in the acceleration nozzle studied is the large reduction in bulk enthalpy attributable to wall heat transfer in the excessive nozzle lengths. This results in low particle exit velocities even though the particles are nearly in velocity equilibrium with the gas. The droplet velocities given here are based on average gas properties; the centerline values will be somewhat higher.

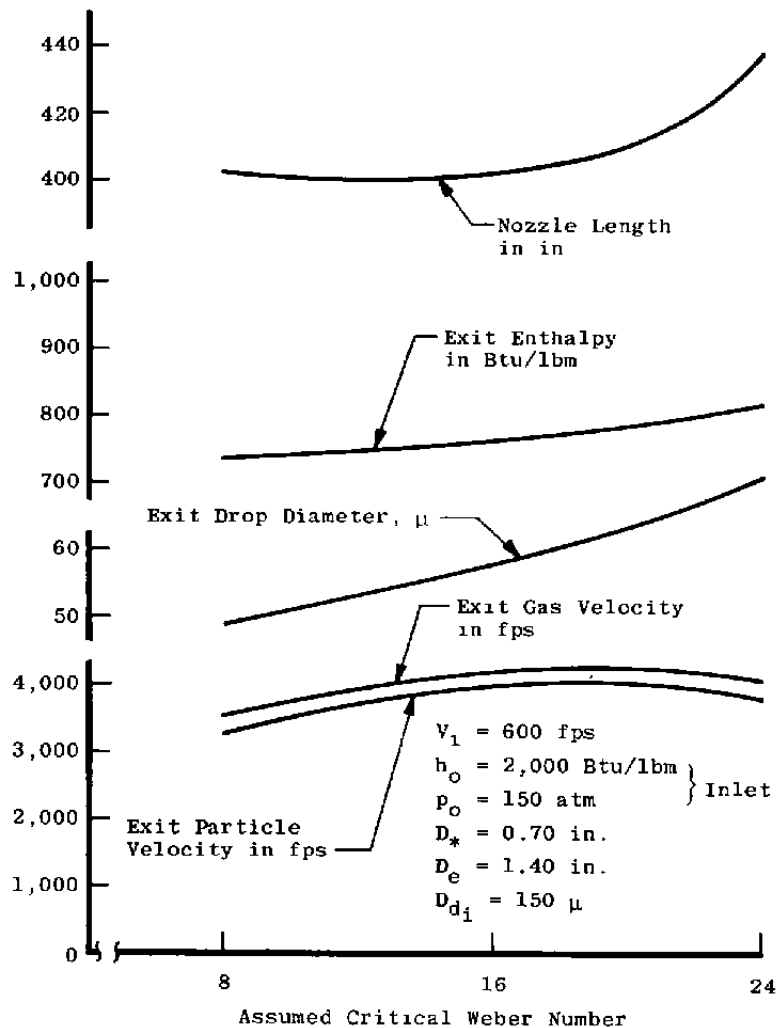


Figure 11. Effect of assumed critical Weber number on the design point performance of droplet acceleration nozzles optimized for the HEAT facility.

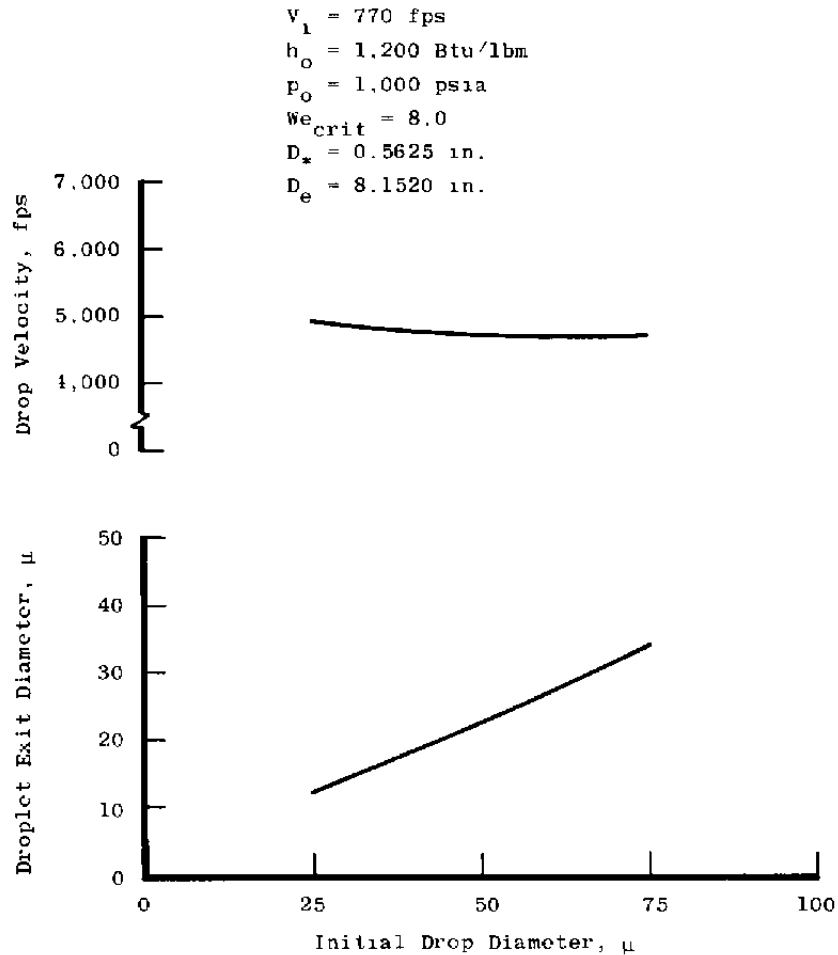


Figure 12. Droplet acceleration performance predictions for modified DET nozzle.

4.3 DROPLET INJECTION

The tentative conclusion that can be made is that high droplet injection velocities are desirable. A droplet injection velocity of 3,000 fps requires an injection pressure of 60,000 psi. Various investigators have used pressure intensifiers to produce high liquid pressures, using a low-pressure gas source. Figure 13 is a sketch of such a device and Fig. 14 illustrates its application to the HEAT facility. The ratio of diameters of the intensifier can be varied to produce pressure ratios of 10:1 or greater. Installing the intensifier and the arc heater adapter required to minimize the friction losses will not be a routine task.

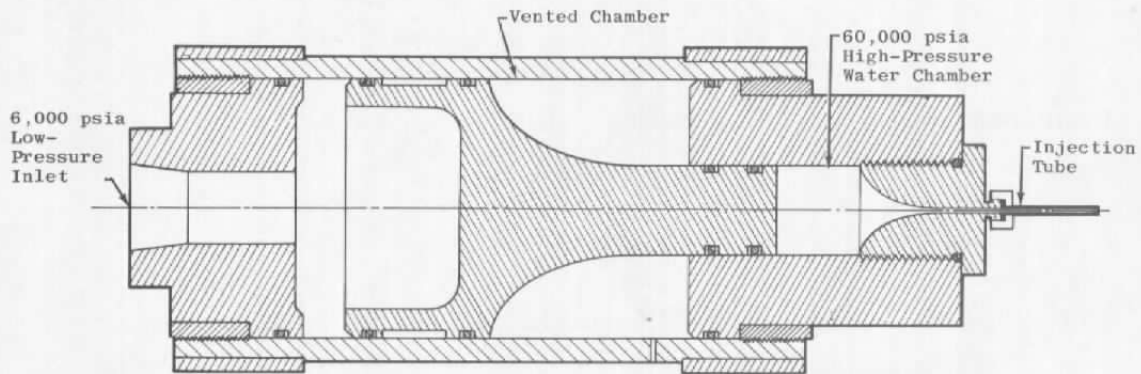


Figure 13. Droplet injection pressure intensifier.

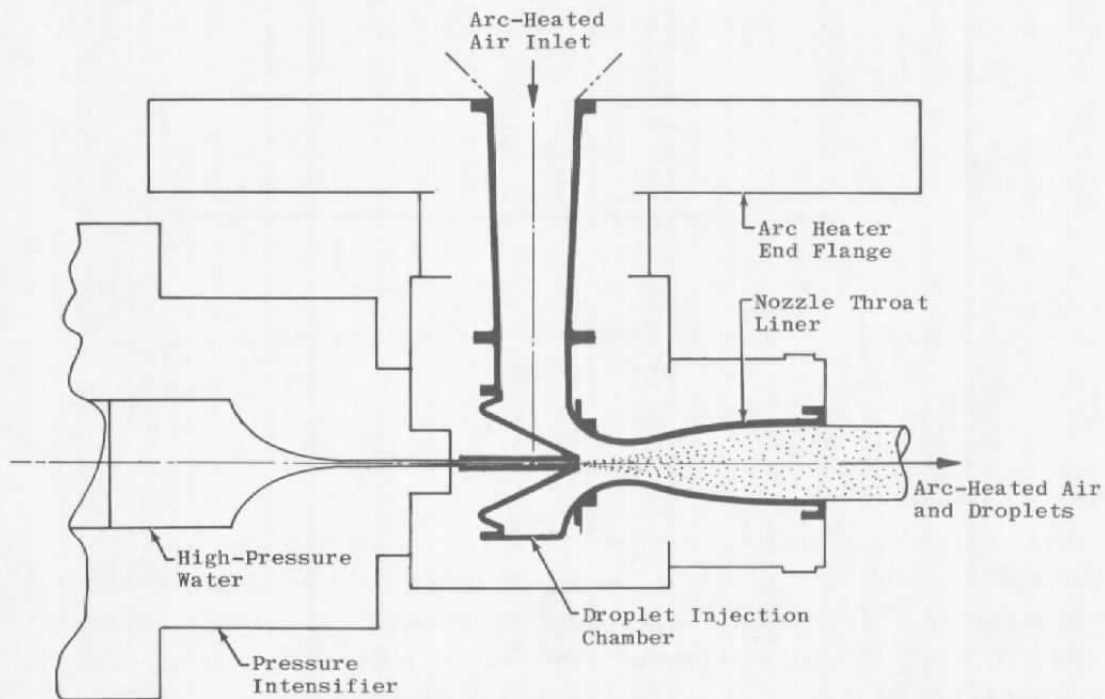


Figure 14. Possible droplet injector/arc heater/acceleration nozzle configuration.

5.0 CONCLUDING REMARKS

1. Although the analyses of the earlier test data were not conclusive, droplet/ice crystal survival in the DET can most probably be attributed to high deformed-droplet drag loads and the resulting high acceleration, which reduced the droplet slip velocity before completion of the breakup process.
2. The method of analysis described in Section 3.1 models all of the important flow phenomena in a high-temperature droplet acceleration nozzle. The water/ice phase transition should be included in the analysis of low-temperature droplet acceleration nozzles such as the DET.
3. Droplet acceleration nozzle contours can be derived to inhibit droplet breakup caused by high Weber number, but these contoured nozzles will be very long and will have high heat-transfer losses to the wall.
4. An erosion field of 35- μ -diameter droplets can probably be achieved in the DET if a new droplet injection chamber and nozzle throat are designed.
5. A droplet erosion field of 150- μ -diameter droplets can probably be produced in the HEAT facility if a new droplet acceleration nozzle throat and high-velocity droplet injection mechanism are developed.
6. Further analytical and experimental work should be done concerning high-velocity droplet injection techniques.
7. The one-dimensional droplet acceleration nozzle code should be modified to include a better wall-heat-transfer model and the water-ice phase change model.
8. A two-dimensional droplet acceleration nozzle code should be developed similar to the solid, particle acceleration nozzle code of Ref. 28 to predict the distribution of droplets across the nozzle exit.
9. A full parametric study of the droplet acceleration nozzle parameters should be made before any future development.

REFERENCES

1. Plank, Vernon G. "Hydrometer Data and Analytical-Theoretical Investigations Pertaining to the SAMS Rain Erosion Program of the 1972-73 Season at Wallops Island, Virginia." AFGL/SAMS Report No. 5; AFGL-TR-77-0149.
2. Barber, John P. "Water Drop Breakup/Impact Damage Threshold." AFML-TR-76-126 (AD-A032429), July 1976.
3. *Test Facilities Handbook*. Eleventh Edition, Parts 6 and 7. Arnold Engineering Development Center, Arnold Air Force Station, Tennessee, June 1979.
4. Reitz, R. D. and Bracco, F. V. "Ultra-High-Speed Filming of Atomizing Jets." *Physics of Fluids*, Vol. 22, No. 6, June 1979, pp. 1054-1064.
5. Putnam, A. A., Benington, F., Einbinder, H., et al. "Injection and Combustion of Liquid Fuels." WADC-TR-56-344, March 1957.
6. Wolfe, H. E. and Andersen, W. H. "Kinetics, Mechanism, and Resultant Droplet Sizes of the Aerodynamic Breakup of Liquid Drops." Aerojet-General Corporation, Report 0395-04 (18) SP (AD437340), April 1964.
7. Ingebo, Robert D. "Maximum Drop Diameters for the Atomization of Liquid Jets Injected Concurrently into Accelerating or Decelerating Gas Streams." NASA TN-D-4640, July 1968.
8. Fewell, K. P. and Kessel, P. A. "Analysis, Design, and Testing of Components of a Combined Ablation/Erosion Nozzle." AEDC-TR-75-154 (AD-A021963), March 1976.
9. Reinecke, W. G. and Waldman, G. D. "Shock Laser Shattering of Cloud Drops in Re-entry Flight." AIAA Paper 75-152.
10. Swain, C. E. and Webber, W. T. "Particle/Shock Layer Interaction in Hypersonic Re-entry." AIAA Paper 75-110.
11. Harper, E. Y., Grube, G. W., and Chaney, I. D. "The Deformity and Instability of a Suddenly Accelerated Liquid Drop." AIAA Paper 71-393.

12. Soo, Shao-lee. *Fluid Dynamics of Multiphase Systems*. Blaisdell Publishing Company, Waltham, Massachusetts, 1967.
13. Rudinger, G. "Gas-Particle Flow in Convergent Nozzles at High Loading Ratios." *AIAA Journal*, Vol. 8, No. 7, July 1970, pp. 1288-1294.
14. Huebner, A. L. "The Effect of Charge Transport on the Disintegration of Liquid Jets." Rocketdyne Division of North American Rockwell Corporation, R7487 (AD673860), May 1968.
15. Elliot, D. G. and Weinberg, E. "Acceleration of Liquids in Two-Phase Nozzles." JPL/CIT TR-32-987, July 1968.
16. Hughes, R. R. and Gilliland, E. R. "The Mechanics of Drops." *Chemical Engineering Progress*, Vol. 48, No. 10, October 1952, pp. 497-504.
17. Ingebo, Robert D. "Drag Coefficients for Droplets and Solid Spheres in Clouds and Accelerating in Airstreams." NACA-TN-3762, September 1956.
18. Tam, Christopher K. W. "The Drag on a Cloud of Spherical Particles in Low Reynolds Number Flow." *Journal of Fluid Mechanics*, Vol. 38, Part 3, September 1969, pp. 537-546.
19. Agosta, V. D. and Hammer, S. S. "Vaporization Response of Evaporating Drops with Finite Thermal Conductivity." NASA-CR-2510, January 1975.
20. Brahinsky, Herbert S. and Neel, Charles A. "Tables of Equilibrium Thermodynamic Properties of Air, Vol. II, Constant Pressure." AEDC-TR-69-89 (AD686410), April 1969.
21. Keenan, Joseph Henry and Keyes, Frederick K. *Thermodynamic Properties of Steam Including Data for the Liquid and Solid Phases*. Second printing. John Wiley and Sons, Inc., New York, 1964.
22. Bird, Robert B., Stewart, Warren E., and Lightfoot, Edwin N. *Transport Phenomena*. John Wiley and Sons, Inc., New York, 1960.
23. Dorsey, N. E., compiler. *Properties of Ordinary Water-Substance in All Its Phases: Water-Vapor, Water and All the Ices*. Reinhold Publishing Company, New York, 1940.

24. Rohsenow, Warren M. and Choi, Harry Y. *Heat, Mass, and Momentum Transfer*. Prentice-Hall, Inc., Englewood Cliffs, New Jersey, 1961.
25. Weast, Robert C. *Handbook of Chemistry and Physics*. 51st edition. The Chemical Rubber Company, Cleveland, Ohio, 1970.
26. Hansen, Arthur G. *Fluid Mechanics*. John Wiley and Sons, Inc., New York, 1967.
27. Narkis, Yahli and Gal-Or, Benjamin. "Minimum Evaporation in Two-Phase Flows." *International Journal of Heat and Mass Transfer*, Vol. 18, No. 7/8, July-August 1975, pp. 845-848.
28. Kessel, P. A. "A Study of the Aerodynamic Design of Viscous Nozzles Used to Accelerate Large Particles to High Velocity." Ph.D. Dissertation, University of Tennessee, Knoxville, March 1977.

APPENDIX

DERIVATION OF TWO-PHASE FLOW CONSERVATION EQUATIONS

The equations of conservation of mass, momentum, and energy used in this study are derived below for one-dimensional two-phase compressible flow of a real equilibrium gas and evaporating liquid droplets including the effects of momentum and energy exchange between the gaseous phase and the wall and the gaseous phase and the droplets.

The global continuity equation is obtained by noting

$$\dot{m}_g = \dot{m}_{nc} + \dot{m}_v$$

$$\frac{d\dot{m}_g}{dx} = \frac{d\dot{m}_{nc}}{dx} + \frac{d\dot{m}_v}{dx}$$

since

$$\frac{d\dot{m}_{nc}}{dx} = 0$$

$$\frac{d\dot{m}_v}{dx} = -\frac{d\dot{m}_c}{dx}$$

then

$$\frac{d\dot{m}_g}{dx} = -\frac{d\dot{m}_d}{dx}$$

From the basic continuity relationship $\dot{m}_g = \rho u A$, it follows that

$$\dot{m}_g \left(\frac{1}{\rho} \frac{d\rho}{dx} + \frac{1}{u} \frac{du}{dx} + \frac{1}{A} \frac{dA}{dx} \right) = -\frac{d\dot{m}_d}{dx} \quad (A-1)$$

where A is taken to be the total nozzle flow area, thus assuming that the droplets have no volume. By defining a real-gas state parameter for the mixture, \bar{R} , as

$$\bar{R} = \frac{p}{\rho h}$$

and noting that

$$A = \frac{\pi}{4} D_N^2$$

expression (A-1) becomes

$$\frac{1}{u} \frac{du}{dx} - \frac{1}{h} \frac{dh}{dx} - \frac{1}{\bar{R}} \frac{d\bar{R}}{dx} + \frac{1}{p} \frac{dp}{dx} + \frac{2}{D_N} \frac{dD_N}{dx} = - \frac{\dot{m}_d}{\dot{m}_g} \frac{3}{D_d} \frac{dD_d}{dx} \quad (A-2)$$

The momentum equation follows from Newton's Second Law; i.e., the change in momentum is equal to the sum of the external forces applied to an infinitesimal element:

$$dF = d(\dot{m}_g u + \dot{m}_d V_d)$$

$$dF = \dot{m}_g du + (V_d - u) d\dot{m}_d + \dot{m}_d dV_d$$

since

$$d\dot{m}_g = -d\dot{m}_d$$

since

$$dF = A dp + \pi D_N \tau_w dx$$

then

$$\dot{m}_g du + (V_d - u) d\dot{m}_d + \dot{m}_d dV_d = A dp - \pi D_N \tau_w dx$$

$$\frac{du}{dx} + \frac{(V_d - u)}{\dot{m}_g} \frac{d\dot{m}_d}{dx} + \frac{\dot{m}_d}{\dot{m}_g} \frac{dV_d}{dx} = - \frac{A}{\dot{m}_g} \frac{dp}{dx} - \frac{\pi D_N \tau_w}{\dot{m}_g}$$

since

$$\dot{m}_g = \frac{\pi D_N^2}{4} \rho u$$

$$\tau = \frac{\rho u^2}{2} C_f \quad (A-3)$$

$$\frac{1}{\dot{m}_d} \frac{d\dot{m}_d}{dx} = \frac{3}{D_d} \frac{dD_d}{dx}$$

then

$$\frac{du}{dx} + \frac{A}{\dot{m}_g} \frac{dp}{dx} + \frac{\dot{m}_d}{\dot{m}_g} \frac{dV_d}{dx} - \frac{3 \dot{m}_d}{\dot{m}_g} \frac{(u - V_d)}{D_d} \frac{dD_d}{dx} = - \frac{2u C_f}{D_N} \quad (A-4)$$

The energy equation results from the simple observation that for a flowing system

$$\frac{d}{dx} \left[\dot{m}_g \left(h + \frac{u^2}{2} \right) + \dot{m}_d \left(C_{p_d} T_d + \frac{V_d^2}{2} \right) \right] = \frac{dQ_w}{dx}$$

Performing the differentiation and noting that

$$\frac{dQ_w}{dx} = \pi D C_h \rho u (h_w - h_o)$$

it proceeds directly that

$$\begin{aligned} \frac{dh}{dx} + u \frac{du}{dx} + \left(C_{p_d} T_d + \frac{V_d^2}{2} - h - \frac{u^2}{2} \right) \frac{\dot{m}_d}{\dot{m}_g} \frac{1}{\dot{m}_d} \frac{d\dot{m}_d}{dx} \\ + \frac{\dot{m}_d}{\dot{m}_g} C_{p_d} \frac{dT_d}{dx} + T_d \frac{dC_{p_d}}{dx} + V_d \frac{dV_d}{dx} = \frac{4 C_h (h_w - h_o)}{D_N} \end{aligned}$$

Assuming

$$\frac{dC_{p_d}}{dx} = 0$$

and applying expression (A-3) it follows that

$$\begin{aligned} u \frac{du}{dx} + \frac{dh}{dx} + \frac{\dot{m}_d}{\dot{m}_g} \left(V_d \frac{dV_d}{dx} + C_{p_d} \frac{dT_d}{dx} \right) + 3 \frac{\dot{m}_d}{\dot{m}_g} \frac{1}{D_d} \frac{dD_d}{dx} \left(C_{p_d} T_d + \frac{V_d^2}{2} - h - \frac{u^2}{2} \right) \\ = - \frac{4C_h}{D_N} (h_o - h_w) \end{aligned} \quad (A-5)$$

NOMENCLATURE

A	Cross-sectional area
a	Gas stream acceleration
A_c	Gas stream acceleration to surface tension ratio
B_o	Bond number
C_d	Droplet drag coefficient
C_f	Shear stress coefficient
C_h	Stanton number
C_p	Specific heat
C_q	Flow discharge coefficient
D	Diameter
D_{ab}	Molecular diffusion coefficient
Δx	Increment in x
F	Force
g	Gravitational constant
h	Specific enthalpy
h_f	Film heat-transfer coefficient
k	Thermal conductivity
K_g	Mass-transfer coefficient
M	Mach number
m	Mass
\dot{m}	Mass flow rate
M_v	Molecular weight of vapor
Nu	Nusselt number for heat transfer

Nu'	Nusselt number for mass transfer
p	Pressure
Pr	Prandtl number
Q	Normalized droplet surface dynamic pressure, total heat-transfer rate
q	Dynamic pressure
\dot{q}	Heat-transfer rate per unit area
\bar{R}	Real-gas parameter = $P/\rho h$
r	Radius
Re	Reynolds number
R_u	Universal gas constant
S	Surface area
Sc	Schmidt number = $\mu/Dab\rho$
T	Normalized droplet time, temperature
t	Time
u	Gas velocity
V	Droplet velocity
Vol	Volume
We	Weber number
X	Nozzle length coordinate
γ	Ratio of specific heats
δ	Delta or differential
ϵ	Particle volume fraction
λ	Latent heat of vaporization
μ	Micron, micrometer, viscosity
ρ	Specific mass density

σ	Surface tension
τ	Shear
ϕ	Wall angle

SUBSCRIPTS

am	Apparent mass
B	Bulk
b	Breakup
Ba	Bassett
body	Denotes body
d	Drop
g	Gas
gr	Gradient
i	Initial
l	Liquid
m	Average or mean
Max	Maximum
N	Nozzle
nc	Noncondensable
o	Total
p	Surface pressure
OR	Orifice
r	Relative
S	Stokes
s	Surface

t	Tip
v	Vapor
w	Wall
∞	Infinity